

# REMEDICATION OF MSW (MUNICIPAL SOLID WASTE) FLYASH AND ITS VALUE-ADDED CONVERSION INTO A GLASS-CERAMIC MATERIAL

*Zaid Ghouleh<sup>\*†</sup>, Mihaiela Isac<sup>†</sup>, Pierre Carabin<sup>◇</sup>, Janusz A. Kozinski<sup>•</sup>, Roderick I.L. Guthrie<sup>†</sup>*

<sup>†</sup> McGill University, McGill Metals Processing Centre (MMPC)  
3610 University Street, Montreal, Canada, H3A 2B2  
[zaid.ghouleh@mcgill.ca](mailto:zaid.ghouleh@mcgill.ca); [mihaiela.isac@mcgill.ca](mailto:mihaiela.isac@mcgill.ca); [rod@mmpc.mcgill.ca](mailto:rod@mmpc.mcgill.ca)

<sup>◇</sup> PyroGenesis Canada Inc.  
1744 Williams, Suite 200, Montreal, Quebec, Canada, H3J 1R4  
[pcarabin@pyrogenesis.com](mailto:pcarabin@pyrogenesis.com)

<sup>•</sup> College of Engineering, University of Saskatchewan  
57 Campus Drive, 3B48 Engineering Building, Saskatoon, SK, Canada, S7N 5A9  
[janusz.kozinski@usask.ca](mailto:janusz.kozinski@usask.ca)

CORRESPONDING AUTHOR: Zaid Ghouleh  
Email: [zaid.ghouleh@mcgill.ca](mailto:zaid.ghouleh@mcgill.ca); [zaid.ghouleh@gmail.com](mailto:zaid.ghouleh@gmail.com)  
Tel (office): 514-398-4755 ext. 09522  
Tel (mobile): 514-570-8634

## **ABSTRACT**

This study sets out to investigate the morphological transformations that occur during the remedial conversion of toxic MSW (Municipal Solid Waste) Incinerator fly ash into an environmentally stable glass-ceramic material. It presents an elaborate characterization approach that: 1) details the devised heat treatment process, 2) identifies the crystalline phases that emerge in the final glass-ceramic composite structure and, 3) employs, perhaps for the first time, state-of-the-art CLSM (Confocal Laser Scanning Microscopy) technology for in-situ real-time observation of the microstructural changes that occur. The conversion of fly ash into a glass-ceramic was achieved through a two-stage heat treatment process involving, first, a vitrification stage that yields a vitreous material via melting and subsequent rapid quenching, and, secondly, a controlled crystallization stage that converts the vitreous material into a glass-ceramic. Crystallographic analysis was carried out by means of XRD and EBSD (Electron Back Scattered Diffraction), both of which concluded that Nepheline and Diopside are the two crystalline phases that form in the final product, with Nepheline being the predominant phase. These findings were complemented by DTA, SEM, and FactSage® analyses. Additionally, experimental observations suggested that high temperature reactions were taking place between the crucible and the fly-ash-slag during melting, an effect believed to influence the characteristics of the final glass-ceramic product. The glass-ceramic obtained in this study seems very promising for future use in structural applications as preliminary appraisal indicates exceptional chemical and dynamical stability – aspects being investigated in an ongoing parallel study.

## **KEYWORDS**

Remediation; Recycling; Toxic-waste; Incinerator Fly-Ash; Vitrification; Controlled-crystallization

## 1. INTRODUCTION

The turn of the 20<sup>th</sup> Century has undoubtedly been accompanied with many positive improvements in the lives of humans. Standards of living have been enhanced, average life expectancy is on the rise, and accelerated scientific understanding has opened doors to endeavors that once seemed impossible. Along with these remarkable trends, however, is a rapid increase in the generation of wastes associated with increased populations and consumerism.

The United Nations and other agencies estimate current worldwide MSW (Municipal Solid Waste) production to range between 1 and 1.3 billion tons per year [1]. The environmental concern with MSW production is that the majority of this waste reports to landfills. Although practical and inexpensive, the practice of landfilling has serious environmental repercussions. These include: GHG (Green House Gas) and odour emissions, and soil & water contamination due to landfill leachate [2, 3]. It also involves the occupation of vast stretches of land, hence, posing difficulty for regions with high population densities and limited disposal spaces. Increased environmental awareness and geographic challenges pose serious constraints for this practice.

Incineration is a favored alternative to landfilling, and a far more effective mode of waste handling. It entails the thermal combustion of MSW, and is capable of achieving 90% volume reduction of the initial waste [3, 4]. On the downside, however, incineration generates considerable amounts of unstable by-products, namely, fly ash and bottom ash residues. The toxic nature of these residues and their subsequent handling methods are topics of much debate, especially for fly ash.

Fly ash is considered more hazardous on account of its finer size and highly toxic constituents. When landfilled, it can inflict adverse ecological and environmental effects. “[It’s] management [is] one of the most important environmental issues related to the incineration of MSW” [5]. It is classified as toxic primarily as a result of containing high levels of leachable heavy metals. Its other toxic constituents include organic contaminants such as Volatile Organic Compounds (VOCs), Polycyclic Aromatic

Hydrocarbons (PAHs), dioxins, and furans [5, 6]. Increased environmental awareness has led a number of countries to prohibit the landfilling of untreated fly ash. Therefore, fly ash is required to undergo further inertisation treatment prior to being dumped in landfills.

Of the different techniques proposed for fly ash handling, thermal stabilization is one of the most promising since it achieves effective containment of the fly ash. Vitrification is one such thermal treatment, and has been adopted worldwide. During vitrification, the fly ash becomes rid of nearly all its hazardous components; while its heavy metals become entrapped in the final product. In addition, the high temperatures typical of this process destroys 99.9% of the fly ash's organic contaminants [7, 8]. The MSW fly ash's composition enables one to obtain an inert, fully amorphous material upon vitrification, i.e. melting and rapid cooling. It largely comprises  $\text{SiO}_2$ ,  $\text{Al}_2\text{O}_3$ , and  $\text{CaO}$ , and, typically, falls within the margins of the  $\text{CaO-Al}_2\text{O}_3\text{-SiO}_2$  (CAS) ternary glass system. The amorphous product obtained from vitrification is very stable and can be safely disposed of in landfills, or, as some studies suggest, used as raw materials for certain applications [3, 8].

The further use of this vitreous product in building and construction is debated by many on the premise that this material lacks sufficient mechanical characteristics that allow its safe use. Individual studies by Boccaccini and Nishida deem these products unsuitable for use in civil engineering works [9] & [10]. Complementing studies indicate that these products have limited applications and are normally landfilled with no economic benefit. Moreover, vitrification is an energy-intensive process that can prove to be costly. It can be more justified if a value-added material with suitable mechanical properties and a high market value can be produced, thereby, offsetting the cost of fabrication. The promising chemical composition of MSW fly ash makes pursuing the production of glass-ceramics seem feasible and the subject of much ongoing research.

The amorphous product obtained from vitrification could be converted into a more durable glass-ceramic material by means of a controlled crystallization heat treatment. The two-stage heat treatment is designed to induce both nucleation and crystallization [7]. Nucleation is the first stage and involves the formation of stable nuclei within the glass matrix. It is prompted when appropriate thermal conditions

are reached. The subsequent crystallization stage, carried out at a higher temperature, promotes crystal growth and the formation of a new crystalline phase [11, 12]. The outcome is a glass-ceramic material with randomly oriented crystals embedded in a residual glass matrix [13]. Glass-ceramics, in general, are known to exhibit good dimensional stability, superior mechanical strength, high abrasion resistance, and notable chemical durability [14]. The heat treatment devised and the types of crystalline phase(s) obtained in the final glass-ceramic product are highly dependant on the fly ash's initial composition.

## **2. EXPERIMENTAL SECTION**

The fly ash used in this study was supplied by the Quebec City Municipal Solid Waste Incinerator located in Quebec, Canada. Melting was carried out in a THERMOLYNE F46240 resistance furnace under atmospheric conditions. The fly ash was compacted into a high-purity alumina (> 99%) casting crucible and heated to 1500°C, where it was held at that temperature for 2 hours. The melt was then quenched in water at room temperature to form glassy granules, referred to herein as the “vitreous material.” The vitreous material was then converted into a glass-ceramic by submitting it to a multi-step heat treatment. The fly ash, vitreous, and glass-ceramic, materials were all then subject to extensive analysis and comparative appraisals. Brief descriptions of these techniques and equipment are mentioned in this section.

The chemical compositions of the fly ash, vitreous, and glass-ceramic materials were determined from XRF (X-Ray Fluorescence) analysis performed using a PANALYTICAL PW2440 Spectrometer (MagiX PRO Series). Sulphur and Carbon contents of the fly ash were measured by means of an ELTRA CS-800 Carbon/Sulfur Analyzer. Loss on Ignition (LOI) was measured in accordance with ASTM standards - ASTM D7348-07.

DTA (Differential Thermal Analysis) was carried out on the vitreous sample using a PERKIN ELMER DTA-7 machine. The purging gas was argon, and the analysis spanned from room temperature to 1350°C at a heating rate of 10°C/min.

Crystallographic analysis was performed via XRD (X-Ray Diffraction) and EBSD (Electron Back Scatter Diffraction). XRD analysis had been carried out using a PHILIPS PW-1050/65 powder diffractometer with a  $2\theta$  scan range between 10° and 100°. Spectrum matching was conducted using the accompanied PANalytical X'Pert HighScore software. Identification of crystalline phase(s) was with reference to the ICDD (International Centre for Diffraction Data) database. EBSD analysis was performed using a PHILIPS XL30 FE-SEM. Scanning was conducted at a magnification of x1000 over an area of 17220  $\mu\text{m}^2$  with a scan step-size of 0.25  $\mu\text{m}$ . Sample preparation necessitated the use of a BUEHLER VIBROMET vibratory polisher to ensure that the samples were completely flat and had a near-mirror finish surface.

The microstructure and its evolution during heating were studied using SEM and CLSM (Confocal Laser Scanning Microscopy). A PHILIPS XL30 FE-SEM operating at an accelerating voltage of 15kV was used for the surface characterization of the glass-ceramic material produced. The sample was etched with a 5% HF acid solution for 30 seconds and then coated with a thin layer of Au-Pd prior to analysis. The confocal laser microscope used was a LASERTEC 1LM21-SVF17SP that allows ultra high temperature *in-situ* observation and real-time recording. The regime selected was a simulation of the devised controlled-crystallization heat treatment, which included holding times of 60min at 805°C, 30min at 905°C, and 30min at 990°C. For this analysis, a lengthy sample preparation was required to ensure that the sample was: perfectly flat from both adjacent sides, had a thickness between 1mm and 3mm, had a diameter not exceeding 8mm, and was polished to a near-mirror finish.

Finally, equilibrium thermodynamic simulation was carried out using FactSage® 5.5 Thermochemical software. Justifiable modifications were made to the composition of the fly ash in order to obtain valid extrapolations.

### 3. RESULTS AND DISCUSSION

#### 3.1. Compositional Analysis and Loss on Ignition (LOI)

The compositions of the fly ash, the vitreous, and the glass-ceramic materials are presented in Table 1. Major components are expressed in their most probable oxide form, and their compositions are given in weight %. Trace components, on the other hand, are presented in elemental form and have values of ppm (mass units). The standard deviation of the values associated with the fly ash help exemplify the material's variability in composition. This variability is directly linked to the disposal trends practiced by the local population being served by the incinerator. The composition of fly ash may vary from season to season and year to year. Therefore, it is worth noting that the batch used in this research study was collected in October of 2007. The LOI value obtained for the fly ash was 7.12%. This loss in weight is attributed to the vaporization of moisture and/or chlorine, and the oxidation of carbon, sulphur, and other volatiles.

Table 1: Composition of the Fly Ash, Vitreous, and Glass-ceramic samples obtained from XRF analysis (major oxides are expressed in wt% while trace components are given in mass ppm).

Major Components	Weight % (DL = 0.01)			Trace Components	ppm (DL = 100)		
	Fly Ash	Vitreous	Glass-ceramic		Fly Ash	Vitreous	Glass-ceramic
SiO <sub>2</sub>	24.26 ± 3.97	34.97	34.18	Ag	566 ± 127	-	-
TiO <sub>2</sub>	3.11 ± 0.51	2.34	2.46	Ba	1512 ± 408	929	2265
Al <sub>2</sub> O <sub>3</sub>	11.94 ± 0.20	30.93	30.47	Br	1540 ± 283	-	-
Fe <sub>2</sub> O <sub>3</sub>	5.24 ± 0.38	5.22	5.53	Cd	150 ± 2	-	-
MnO	0.12 ± 0.01	0.16	0.17	Cr	910 ± 236	846	1066
MgO	2.44 ± 0.45	1.57	1.48	Cu	1429 ± 310	993	1387
CaO	26.82 ± 4.16	16.58	17.20	F	4129	-	-
Na <sub>2</sub> O	5.05 ± 0.50	2.69	2.68	Ni	243 ± 58	299	336
K <sub>2</sub> O	4.04 ± 0.64	1.63	1.61	Pb	2277 ± 502	1372	1494
P <sub>2</sub> O <sub>5</sub>	4.69 ± 0.13	2.32	2.28	Sb	2175 ± 520	674	1371
Cl	7.12 ± 2.17	0.23	0.22	Sn	1133 ± 524	604	709
S	2.25	-	-	Sr	607 ± 133	399	432
C	4.44	-	-	Zn	14751 ± 3471	7159	7778
				Zr	597 ± 563	225	235

- : Not tested

The locations of these materials on the CAS ternary diagram are shown in Figure 1(a) (after their main constituents were normalized to 100%). As shown, there is a significant shift in composition between the fly ash and the vitreous material: this shift occurs during vitrification, as indicated by the composition of the vitreous sample, and is presented by a dashed arrow in Figure 1(a) (devitrification, or the subsequent heat treatment, to a glass-ceramic does not exhibit such a pronounced shift}. However, this effect is not believed to be owed to vitrification alone; complex reactions between the molten fly-ash and the crucible walls seem to be taking place at the holding temperature of 1500°C. This speculation is in agreement with experimental observations noted after quenching, where the walls of the crucibles were noticeably thinner in areas that experienced prolonged contact with the slag. This implies that crucible material (alumina) was being eroded from the walls during the melting process and consequently dissolving into the slag. To better understand the reactions that might have took place, FactSage® was used to simulate the melting conditions during vitrification. Figure 1(b) presents the ternary phase diagram generated by FactSage® for the fly ash slag at 1500°C.

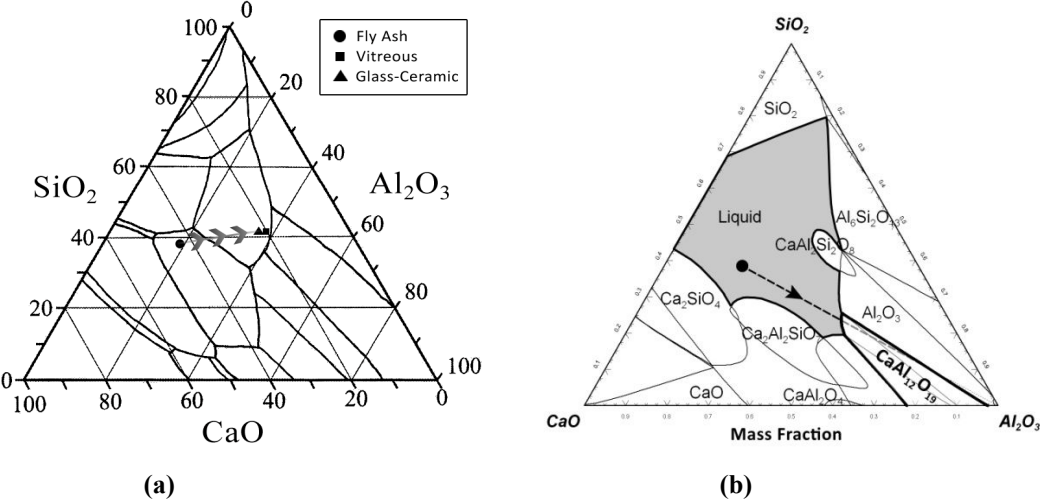


Figure 1: CAS ternary diagram: (a) displaying the compositions of the fly ash, vitreous, and glass-ceramic samples; (b) generated by FactSage® to show the ternary system at the melting temperature of 1500°C.

The simulated ternary diagram (Figure 1(b)) explains the significant and unexpected content increase of  $\text{Al}_2\text{O}_3$ , and decrease of  $\text{CaO}$ , post vitrification. The black dot on the diagram represents the initial composition of the slag. As indicated, it falls within the borders of the liquidus region. The solubility of additional  $\text{Al}_2\text{O}_3$ ,  $\text{CaO}$ , and/or  $\text{SiO}_2$  is very high at this point since none of these components are at the level of saturation in the slag. Being made of high-purity alumina ( $> 99\% \text{Al}_2\text{O}_3$ ), the walls of the crucible act as an infinite source of  $\text{Al}_2\text{O}_3$ . As a result, during the melting at  $1500^\circ\text{C}$ ,  $\text{Al}_2\text{O}_3$  from the walls of the crucible begin to readily dissolve into the slag. It is this dissolution effect that explains the increase in the  $\text{Al}_2\text{O}_3$  content in the vitreous and glass-ceramic products. The change in composition of the slag as more and more  $\text{Al}_2\text{O}_3$  dissolves is traced by a dotted line in the figure. The dissolution of  $\text{Al}_2\text{O}_3$  ceases once the line meets the liquidus. At this point, the slag is saturated with  $\text{Al}_2\text{O}_3$ ; therefore, additional entrainment of alumina into the slag is no longer possible. Nonetheless, the crucible's interaction with the slag does not end there as a subsequent reaction is prompted involving the Ca-oxide content in the slag.

After being partially eroded of  $\text{Al}_2\text{O}_3$ , the walls of the crucible engage in a new thermodynamically-favored reaction that involves the formation of a solid Ca-Al-Oxide phase. The traced line in the simulated ternary diagram (Figure 1(b)) reveals that, beyond the liquidus line, the slag's continual exposure to  $\text{Al}_2\text{O}_3$  from the walls yields a  $\text{CaAl}_{12}\text{O}_{19}$  compound, an outcome of the walls' reaction with  $\text{CaO}$  from the slag. This resultant consumption of  $\text{CaO}$  leads to its relative depletion from the slag and, hence, its reduced weight fraction in the vitreous and glass-ceramic samples (Table 1). Moreover, close examination of the reacted crucible walls reveals that a distinct layer of material is seen deposited along areas that were heavily eroded during melting.

The kinetics of the above-mentioned reactions were not investigated; however, it is believed that there was sufficient time for these reactions to take place since melting prolonged for 2 hours. The referenced study herein had observed a similar occurrence to the latter reaction, where a  $\text{CaAl}_{12}\text{O}_{19}$  compound was formed on the expense of the  $\text{CaO}$  content in a slag having a chemical composition similar to the fly-ash slag being investigated [15]. The study's findings revealed that having a slightly higher  $\text{SiO}_2$  content in

the slag could have avoided the formation of the Ca-Al-oxide compound and, hence, prevented the depletion of CaO from the slag.

### 3.2 Thermal Analysis

The behavior of the vitreous sample during heating can be seen in the DTA plot shown in Figure 2. Thermo-physical changes occurring within the sample can be identified here, along with the temperatures that prompt the mechanisms of nucleation and crystallization. The first apparent feature on the heat curve is that of a shallow endothermic dip with an onset temperature of 730°C. This onset can be ascribed to the glass transition temperature,  $T_g$ . The second small endothermic dip occurs at around 800°C and, based on similar research by T.W. Cheng, is identified as the dilatometric softening point [16]. The two subsequent exothermic peaks, both denoting individual peak crystallization temperatures ( $T_{p1}$  &  $T_{p2}$ ), occur at 893°C and 977°C, respectively. The first crystallization peak is smaller and much less pronounced than the second. The two arrows on the graph mark the temperatures for the respective onsets of crystallization. The first crystallization occurrence in the sample starts at 845°C, while the second is prompted around 935°C. Both crystallization peaks imply physical changes in the sample, or more precisely, the formation of new crystalline phases. Melting appears as a notable endothermic decline, in which complete melting of the sample is achieved by 1181°C.

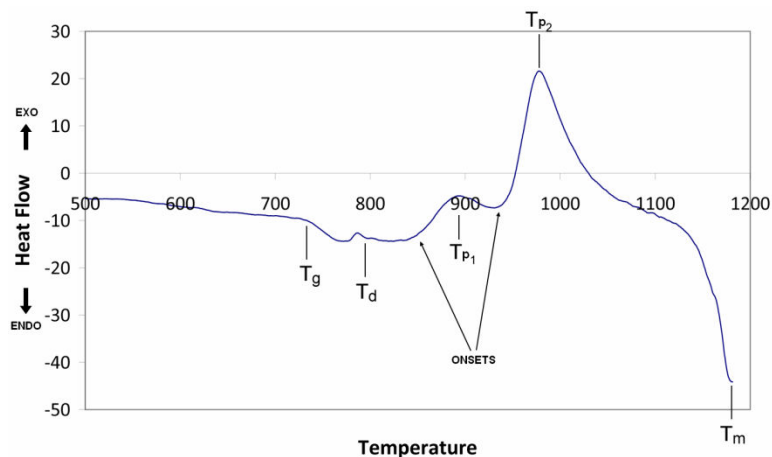


Figure 2: DTA heat curve for the vitreous sample: Glass Transition ( $T_g$ ) 730°C; Dilatometric Softening Point ( $T_d$ ) 793°C; 1<sup>st</sup> Peak Crystallization ( $T_{p1}$ ) 893°C; 2<sup>nd</sup> Peak Crystallization ( $T_{p2}$ ) 977°C; Melting ( $T_m$ ) 1181°C.

### 3.3 Vitreous to Glass-Ceramic Material

From the DTA findings shown above, a heat treatment regime was devised for converting the vitreous material into a durable glass-ceramic product. This four step heat treatment is presented in Figure 3. The selection of the steps was based on the premise that the mechanisms of nucleation and crystallization are prompted by holding the vitreous material at least 10°C above its respective glass transition and peak crystallization temperatures [17]. The heat treatment included a nucleation step at 805°C for 60 minutes, intended for the formation of stable nuclei within the amorphous matrix, followed by two individual crystallization steps at 905°C and 990°C, each lasting 30 minutes. Finally, the samples underwent an annealing step at a temperature of 600°C for a duration of 45 minutes to relieve internal thermal stresses.

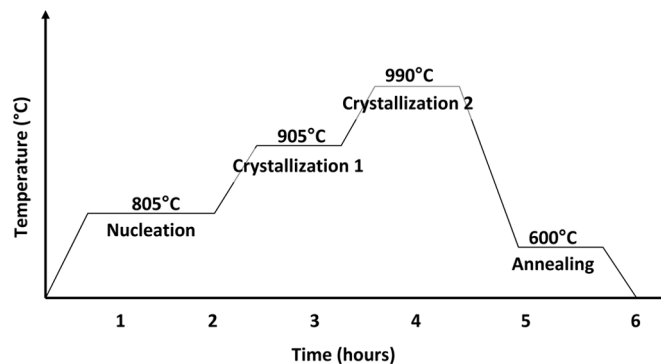


Figure 3: Heat treatment devised for the conversion of the vitreous material into the final glass-ceramic product. It included a nucleation step at 805°C, two crystallizations at 905°C and 990°C, and an annealing step at 600°C.

### 3.4 Crystallographic Analysis

#### 3.4.1 X-Ray Diffraction (XRD)

XRD analysis performed on the glass-ceramic material identified Nepheline and Diopside as the two crystalline phases present in the final product. The results are presented in Figure 4. In order to determine which phase grows first, an additional XRD analysis was performed on the vitreous product after it had only completed the first crystallization step. The resultant spectrum was found to belong to

the Nepheline phase. Hence, the first crystallization peak  $T_{p1}$  observed in the DTA heat curve involves the formation of the Nepheline phase, while  $T_{p2}$  involves that of the Diopside phase. The identified variants of Nepheline and Diopside have the chemical formulae  $\text{Na}_{2.8}\text{K}_{0.6}\text{Ca}_{0.2}\text{Al}_{3.8}\text{Si}_{4.2}\text{O}_{16}$  and  $\text{Ca}(\text{Mg}, \text{Al})(\text{Si}, \text{Al})_2\text{O}_6$ , respectively. In theory, Nepheline is known to have a hexagonal crystal structure, while Diopside belongs to the monoclinic crystal system.

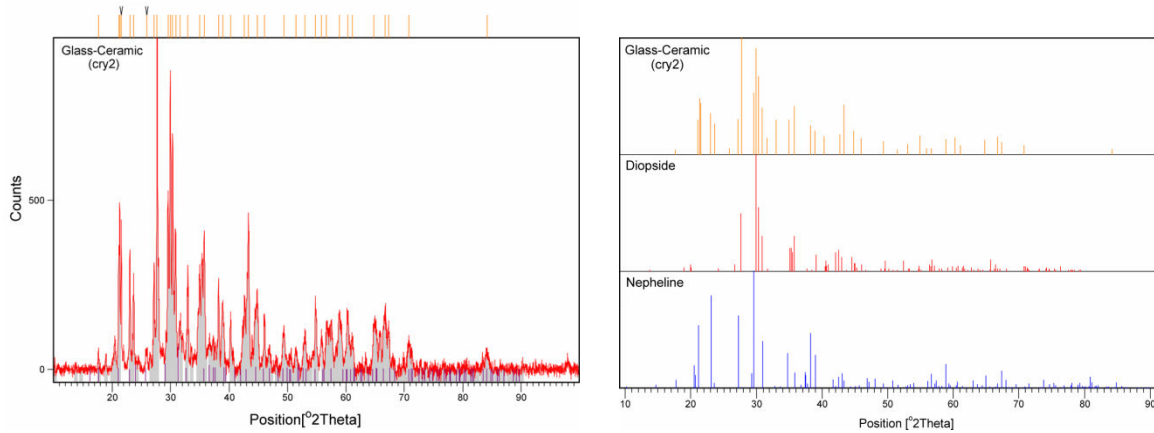


Figure 4: XRD spectrum of the obtained glass-ceramic sample [18]

### 3.4.2 Electron Back Scatter Diffraction (EBSD)

The scan performed to map the predetermined area of the glass-ceramic sample yields the results shown in Figure 5. The image of Figure 5(a) displays fairly defined grain boundaries and crystalline grains belonging to Nepheline and Diopside. Distortions, if any, that may arise in these results could be attributed to interferences from the enveloping residual glass phase, which makes for the remaining non-crystalline portion of the sample. Knowing the crystallographic orientations helps in distinguishing individual grains and in defining their boundaries. To differentiate between the two phases, Figures 5(b) & 5(c) present color-coded images of the Nepheline and Diopside phases, respectively. The different colors identify different crystal orientations, as indicated by the legend. Dark regions in the images reveal areas where the respective crystalline phase was absent.

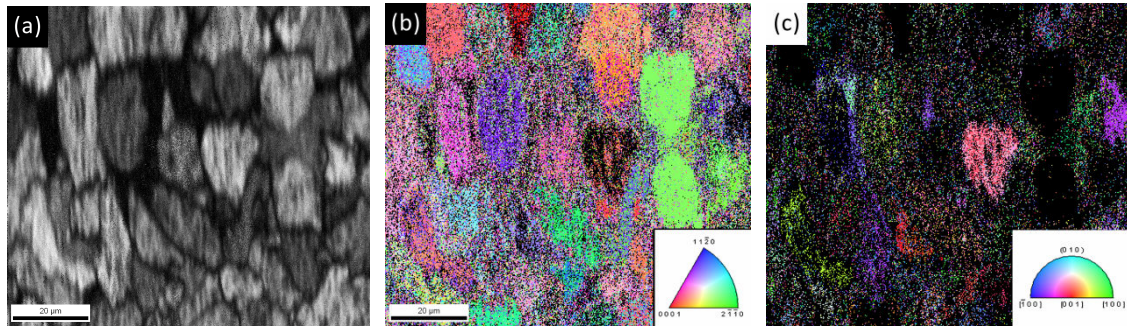


Figure 5: Results obtained from EBSD: (a) Image obtained from crystallographic mapping of the scan area; (b) Image showing individual Nepheline grains and their different orientations; (c) Image for Diopside grains and their different orientations

Figure 5(b) reveals the presence of numerous colored clusters, each believed to represent a single Nepheline grain. The shapes of these grains are not very well-defined, nonetheless, their sizes range between  $20\mu\text{m}$  and  $40\mu\text{m}$  in length. The non-uniform distribution of the colors reveals that the grains are randomly oriented within the sample. The image also reveals that, for the scanned area, Nepheline is the predominant crystalline phase present. The Diopside phase, on the other hand, is present in a much smaller volume fraction, as shown in Figure 5(c). Intense color clusters indicating the presence of individual grains are not observed here. The Diopside phase is scarcely dispersed throughout the scanned area save for a few locations where faint clusters can be observed. This limited presence of Diopside can be attributed to various reasons: 1) The scanned area happens to be arbitrarily overpopulated with the Nepheline phase. 2) The Diopside phase is much smaller than the Nepheline phase, therefore, occupying less volume within the sample. 3) Diopside forms in the bulk of the material (“bulk crystallization”), while Nepheline forms at the surface (“surface crystallization”). 4) The constituents that lead to the formation of the Diopside crystals happen to be present in scarce amounts in the scanned area during the vitreous-to-glass-ceramic heat treatment.

The results obtained for this analysis fit well with earlier findings from XRD. They confirm that the final product obtained from the heat treatments is in fact a semi-crystalline material, with Nepheline and Diopside being the randomly-oriented crystalline phases present. The analysis also indicates that the Nepheline is the more predominant of the phases.

### 3.5 Microstructure Analysis

#### 3.5.1 Scanning Electron Microscopy (SEM)

SEM micrographs for the glass-ceramic material at different magnifications are shown in Figure 6. The darker regions in Figure 6(a) are chasm-like depressions that were once occupied by an amorphous phase prior to being dissolved by the HF etchant. The bright regions are those of the Nepheline phase. In the literature, Nepheline is identified as having a hexagonal crystal structure. Figure 6(b) is taken at a higher magnification and, in addition to Nepheline, it also reveals the presence of the second crystalline phase, Diopside. The Diopside phase forms at a higher temperature (as confirmed from XRD results), and is notably smaller in size. These crystals stretch a couple of microns in length as opposed to the Nepheline crystals, which can extend to more than 20 microns. The small depositions seen covering the surface of the Nepheline crystals are, in fact, remnants of the Diopside phase that had been sliced off during polishing. Figures 6(c) & 6(d) are close up images of the Diopside crystals. As shown, and complemented by the literature, these pillar-like crystals have a monoclinic structure, better described as rectangular prisms with parallelograms for their bases.

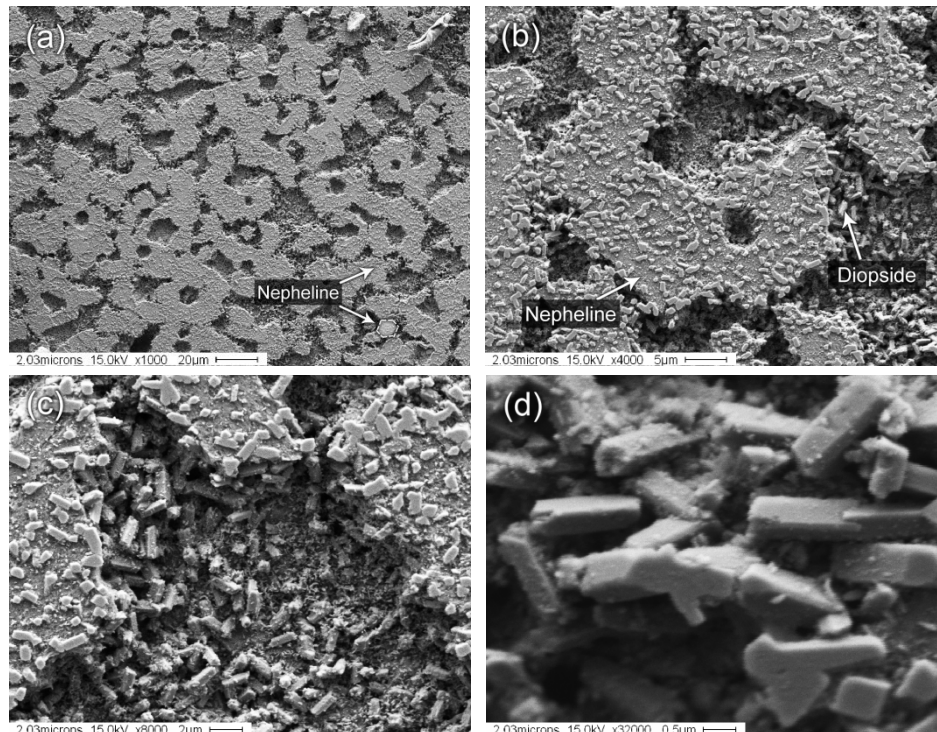


Figure 6: SEM micrographs of the produced glass-ceramic material after completing all steps of the heat treatment. The images are taken at different magnifications, showing crystals of hexagonal Nepheline and monoclinic Diopside: (a) x1000, (b) x4000, (c) x8000, and (d) x32000 [18].

Clear depiction of the structural nature of the Nepheline crystals could not have been demonstrated with the same ease as done for the Diopside crystals. The small size of the Diopside crystals and the manner of their existence in the sample facilitated the task of acquiring clear images of their crystallographic structure. However, SEM is merely a surface characterization technique and is not always expected to reveal features pertaining to the structure of a phase. The results obtained from the XRD analysis herein are regarded as more conclusive in this respect. Also, definitive features of phases can not always be observed since many parameters could affect the final presentation of a sample. Cutting, polishing, acid etching, and coating are all sample preparation techniques that can considerably deform the microstructure.

### *3.5.2 Confocal Laser Scanning Microscopy (CLSM)*

Observation via CLSM gave precise real-time visual interpretation of the thermally-induced physical changes that occur in the sample during the heat treatment. For consistency, the heating regime programmed for this analysis was the same as the one devised to convert the vitreous material into a glass-ceramic (i.e. holding times of 60 min at 805°C for nucleation, 30 min at 905°C for the 1<sup>st</sup> crystallization, and 30 min at 990°C for the 2<sup>nd</sup> crystallization). A fixed area on the surface of the sample was chosen to be examined during the course of heating. Still images of the microstructure were taken at different stages of the heat treatment, and these are shown in Figure 7. The four images presented are snapshots of the monitored surface taken: before commencing the heating (Figure 7(a)), and towards the end of each holding step (Figure 7 (b), (c), & (d)). The images reveal that transformations in the microstructure were occurring at the expected temperatures, thereby confirming findings from previous analyses. These images are not visually synonymous to ones obtained from SEM for reasons pertaining

to different technique capability, beam source, image output, and sample preparation. In addition, CLSM is depth-sensitive and, unlike SEM, depicts results in a 3-dimensional manner.

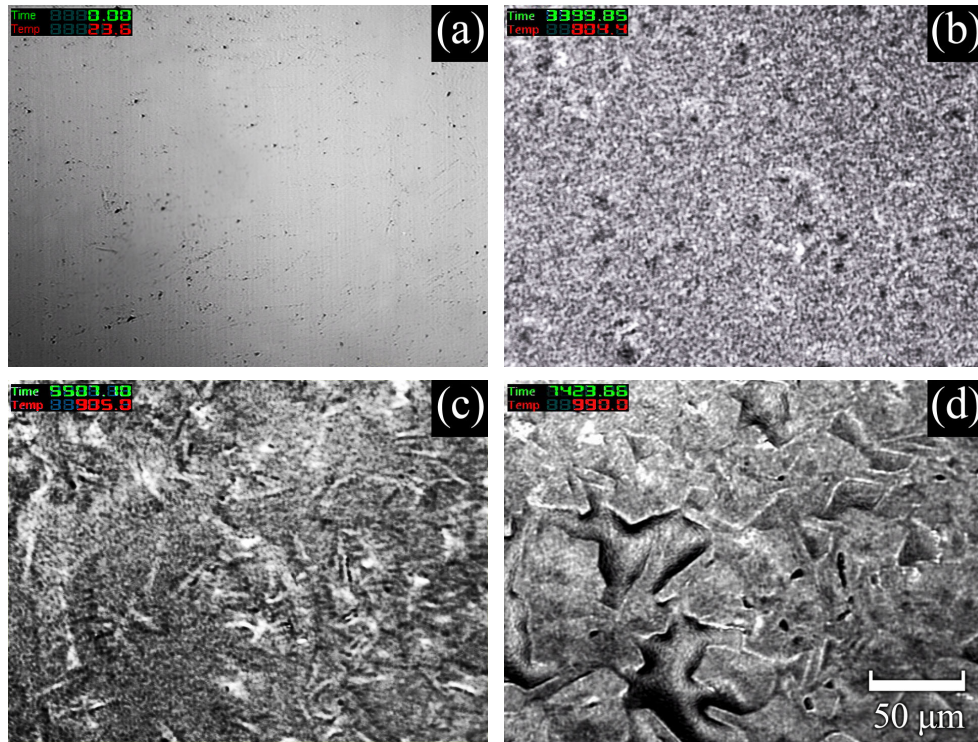


Figure 7: CLSM micrographs showing the progression in the vitreous material's microstructure as it evolves into a glass-ceramic. The images were taken at a magnification of  $\times 1400$ , and at different stages of the multi-step heat treatment: (a) Prior to analysis,  $T = 23.6^{\circ}\text{C}$ , (b) after near completion of the nucleation stage (55<sup>th</sup> minute),  $T = 804.4^{\circ}\text{C}$ , (c) after near completion of the first crystallization stage (29<sup>th</sup> minute),  $T = 905^{\circ}\text{C}$ , and (d) after near completion of the second crystallization stage (30<sup>th</sup> minute),  $T = 990^{\circ}\text{C}$ .

Figure 7(a) is an image of the sample's surface before undergoing heat treatment. At this point, the sample is fully amorphous, with features similar to glass materials. The surface is mostly flat save for some randomly scattered scratches and voids. Figure 7(b) is a picture taken after the sample completed 55 minutes of the scheduled 60 minutes of nucleation. The image reveals that the surface had become coarser, displaying what seems to be troughs and peaks of countless micro protrusions. The surface has a checkered appearance consisting of dark (inward) and bright (outward) spots. Crystalline phases are not observed at this stage of the heat treatment since only microscopic nuclei are expected to form during this holding temperature. The chosen nucleation temperature is believed to be beyond the softening

point of the sample, hence, the sample is expected to be more malleable. This softening effect is a result of the reduction in viscosity with increasing temperature. Experimentally, it had been noted from an out-of-focus flutter that required constant lens adjustment, and a slight expansion evident from a smearing effect at the borders of the monitored region.

In Figure 7(c), more defined crystallographic structures begin to emerge. The image was captured after 29 minutes had elapsed of the 1<sup>st</sup> crystallization stage at 905°C. Previous findings from XRD indicate that the crystalline phase to form at this temperature is Nepheline. Definite structural contours for the Nepheline phase, like ones seen in the SEM images, cannot be observed here since these crystals haven't reached a comparable size yet. The crystals are believed to experience further growth as they are exposed to even higher temperatures during the remaining portion of the heat treatment. In addition, the surface still largely comprises a residual glass phase, which can obstruct the observation of individual crystal geometries.

Figure 7(d) is a snapshot of the sample taken at the very end of the 2<sup>nd</sup> crystallization stage at 990°C (30<sup>th</sup> minute). The image reveals that a noticeable transformation had occurred in the microstructure, one that protracts consistent crystallographic features. Sharp contours of what seem to be crystal edges are clearly visible throughout the surface. These well-defined features are believed to belong to the Nepheline phase; although previous findings indicate that it is the Diopside phase that materializes at this stage of the heat treatment. This is precisely the case. The Diopside crystals do form at this temperature but cannot be observed at this magnification due to their small size (2 – 4 μm), compared to the much larger Nepheline crystals (20 – 40 μm). As expected, the Nepheline phase underwent significant crystal growth at this final holding temperature. Also, as revealed from EBSD, the nature of this phase's presence in the final glass-ceramic is characterized as being randomly-oriented, and overlapping at instances. These features are much more pronounced here since the captured image is sensitive to depth (z-plane). At the bottom left corner of the picture there seems to be an outward bulging effect. This could either be the softened residual amorphous phase being pressured by adjacent crystals growing towards each other, or a result of partial melting of the sample.

CLSM is a powerful characterization technique for observing surface phenomena, but does not deliver the same effectiveness for crystallography. Not being able to observe definite hexagonal features for the Nepheline phase was expected. In addition to obstructions from the residual glass phase, parameters such as crystallographic orientations and growth planes need to be considered for such an observation to be made.

### **3.6 Modelling: FactSage® Simulation**

FactSage® was used to simulate the heat treatment regime carried out for the conversion of the vitreous material into a glass-ceramic. The simulation was conducted using the composition of the vitreous material. However, due to the material's complex make-up, and limitations with certain elemental FactSage® databases, certain constituent eliminations had to be made to facilitate calculations. These modifications will ultimately affect the accuracy of the end results, but, nonetheless, will allow the attainment of a very close indicative model. After normalizing to 100 weight %, the composition considered for the simulation was: 37.7% SiO<sub>2</sub>, 33.04% Al<sub>2</sub>O<sub>3</sub>, 17.72% CaO, 5.58% Fe<sub>2</sub>O<sub>3</sub>, 4.62% Na<sub>2</sub>O, and 1.67% MgO.

The controlled heat treatment conducted herein was carried out in air and at atmospheric pressure. The output of the simulation is presented in the plot of Figure 8, and reveals the simulation's predicted crystalline phases that evolve, and eventually decompose, in the vitreous sample during the course of heating to a melt. Seven distinct curves have been identified, each belonging to a respective crystalline phase that exists in the vitreous material between 500°C and 1600°C. The line labeled "slag" denotes the melting of the material, which commences at 1200°C and continues until the sample is completely molten, around 1450°C. The two curves of relevancy to this study are those belonging to the *Clinopyroxene (Diopside)* and *Nepheline* phases. As shown in the plot, Nepheline is by far the most predominant phase present throughout the simulation, and one with the highest weight fraction compared to the collective fractions of the other phases. The Diopside phase, belonging to the family of

Clino-Pyroxenes, only exists in the sample between 750°C and 1000°C. Its formation follows the simultaneous decomposition of the *Spinel* and  $Ca_3Fe_2Si_3O_{12}$  phases shown present in the sample at immediately lower temperatures.

For this study, the particular range of interest in the plot falls between 800°C and 1000°C, since the nucleation and crystallization steps of the devised heat treatment take place within this temperature span (Section 3.3). The simulation shows that four possible phases coexist within this temperature range, and these are: Nepheline, Clino-Pyroxene, Mel (Melilite), and CAFS (Ca-Al-Fe-Silicate). Therefore, based on the presented model, it is very likely that a Nepheline/Diopside-based glass-ceramic is obtained from the same processing route carried out for the vitreous material in this study.

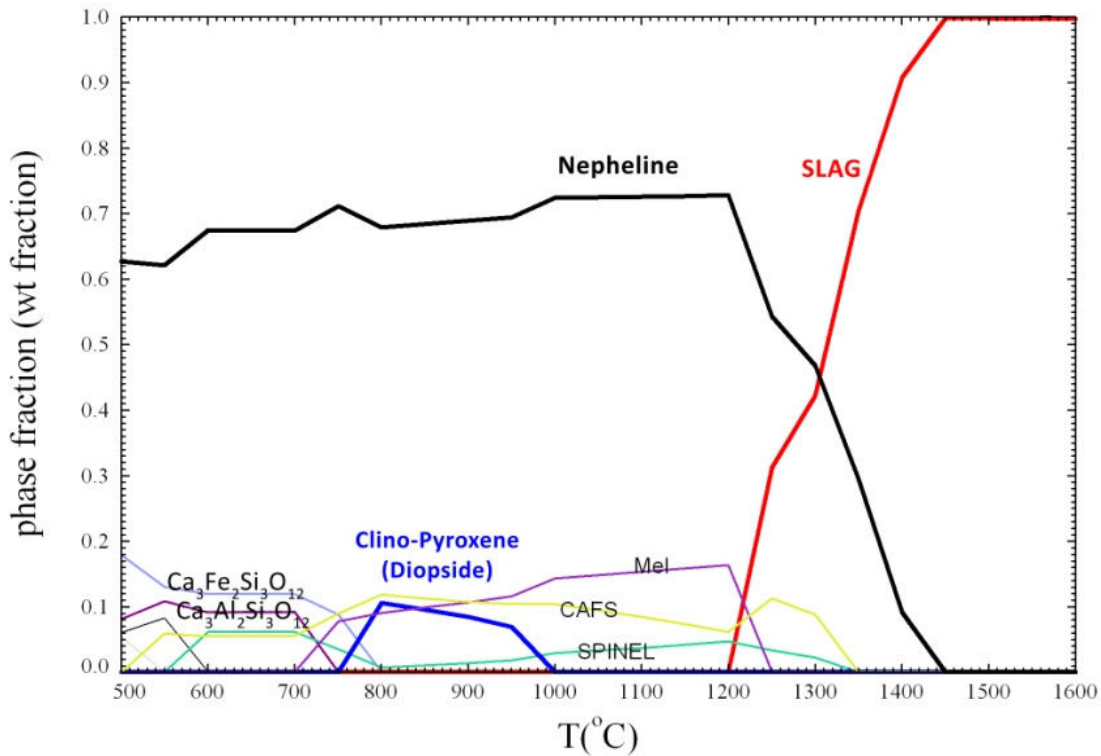


Figure 8: FactSage® results obtained from simulating the heat treatment of the vitreous material into a glass-ceramic. The plot lists the most plausible crystalline phases that form and presents their weight fractions as a function of increasing temperature (from 500°C to 1600°C). **THE SHADED AREA DENOTES THE TEMP RANGE WHERE THE HEAT TREATMENT WAS CARRIED OUT**

The findings obtained from this simulation agree well with physical findings from crystallographic analyses. XRD and EBSD identify the crystalline phases that form as Nepheline and Diopside. EBSD further illustrates that the Nepheline phase is present at much higher concentrations than Diopside in the sample. The results of this simulation asserts that, for the temperatures within which the heat treatment was conducted, it is very likely for the phases of Diopside and Nepheline to form, with a very strong inclination to form more of the Nepheline phase (as shown from its significantly higher weight fraction) than the Diopside.

#### **4. CONCLUDING REMARKS**

This paper successfully demonstrates a high-temperature stabilization method that not only achieves effective containment of the toxic MSW fly ash, but also attains an inert glass-ceramic material for a final product. The glass-ceramic obtained from the devised process route is a homogenous composite material comprised of randomly oriented Nepheline and Diopside crystals embedded within a residual amorphous phase. The Nepheline crystals have hexagonal crystal structures and range between 20 and 40 $\mu$ m in diameter. Alternatively, the Diopside crystals are monoclinic and extend from 2 to 4 $\mu$ m in length. The glass-ceramic granules produced herein exhibit seemingly adequate properties that can promote their consideration as substitutes for structural and building materials, e.g. aggregates. A current study is underway for evaluating/quantifying the chemical and mechanical durability of this material.

## ACKNOWLEDGEMENTS

The authors would like to acknowledge the financial support of NSERC and BIOCAP, and the technical assistance of Dr. Lakshminarayana Rao, Product Development Scientist, PyroGenesis Canada Inc., and Mr. Yves Fréchet, Operations Engineer, City of Quebec, Quebec.

## REFERENCES

1. **Malone R (2006).** "Garbage: World's Worst Waste". Forbes 2006; Available from: [http://www.forbes.com/logistics/2006/05/23/waste-worlds-worst-ex\\_rm\\_0524waste.html](http://www.forbes.com/logistics/2006/05/23/waste-worlds-worst-ex_rm_0524waste.html).
2. **Statistics Canada (2005).** "Human Activity and the Environment: Annual Statistics 2005".
3. **Park Y.J. and J. Heo (2002).** "Vitrification of Fly Ash from Municipal Solid Waste Incinerator". Journal of Hazardous Materials 91(1-3), pp. 83-93.
4. **Ilex Energy Consulting (2005).** "Eligibility of Energy from Waste - Study and Analysis". S.o.S.f.T.a. Industry, UK.
5. **Ferreira C., A. Ribeiro, and L. Ottosen (2003).** "Possible Applications for Municipal Solid Waste Fly Ash". Journal of Hazardous Materials 96(2-3) pp. 201-216.
6. **Millrath K. and N.J. Themelis (2003).** "Waste as a Renewable Source of Energy: Current and Future Practices". ASME *International Mechanical Engineering Congress & Exposition (IMECE)*. Washington D.C.
7. **Rincó J.M., M. Romero, and A.R. Boccaccini (1999).** "Microstructural Characterisation of a Glass and a Glass-ceramic Obtained from Municipal Incinerator Fly Ash." Journal of Materials Science 34(18), pp. 4413-4423.
8. **Cheng T.W. (2004).** "Effect of Additional Materials on the Properties of Glass-ceramic Produced from Incinerator Fly Ashes". Chemosphere 56(2), pp. 127-131.
9. **Boccaccini A. and R. Rawlings (2002).** "Glass-Ceramics from Waste Materials." Materials World 10, pp. 16-18.
10. **Nishida K., et al. (2000).** "Melting and Stone Production Using MSW Incinerated Ash." Waste Management 21(no: 5 (3 ref.)), pp. 443-449.
11. **Erol M., S. Kucukbayrak, and A. Ersoy-Mericboyu (2007).** "Production of Glass-ceramics Obtained from Industrial Wastes by Means of Controlled Nucleation and Crystallization." Chemical Engineering Journal 132(1-3), pp. 335-343.

12. **Karamanov A., M. Pelino, and A. Hreglich (2003).** "Sintered Glass-ceramics from Municipal Solid Waste-Incinerator Fly Ashes--Part I: The Influence of the Heating Rate on the Sinter-crystallization." *Journal of the European Ceramic Society* 23(6), pp. 827-832.
13. **Qian G., et al. (2006).** "Diopside-based Glass-ceramics from MSW Fly Ash and Bottom Ash." *Waste Management* 26(12), pp. 1462-1467.
14. **Peng F., et al. (2004).** "Nano-crystal Glass-ceramics Obtained by Crystallization of Vitrified Coal Fly Ash". *Fuel* 83(14-15), pp. 1973-1977.
15. **Park J.H., I.-H. Jung, and H.-G. Lee (2006).** "Dissolution Behavior of Al<sub>2</sub>O<sub>3</sub> and MgO Inclusions in the CaO-Al<sub>2</sub>O<sub>3</sub>-SiO<sub>2</sub> Slags: Formation of Ring-like Structure of MgAl<sub>2</sub>O<sub>4</sub> and Ca<sub>2</sub>SiO<sub>4</sub> around MgO Inclusions." *ISIJ International* Vol. 46(No.11), pp. 1626-1634.
16. **Cheng T.W. and Y.S. Chen (2003).** "On Formation of CaO-Al<sub>2</sub>O<sub>3</sub>-SiO<sub>2</sub> Glass-ceramics by Vitrification of Incinerator Fly Ash." *Chemosphere* 51(9), pp. 817-824.
17. **Erol M., et al. (2001).** "Crystallization Behaviour of Glasses Produced from Fly Ash." *Journal of the European Ceramic Society* 21(16), pp. 2835-2841.
18. **Ghouleh Z., et al. (2009).** "High Temperature Processing of Fly Ash for the Production of an Environmentally Safe Material," in *MOLTEN2009: 8th International Conference on Molten Slags, Fluxes, and Salts*. Santiago, Chile.